(Article begins on next page)

Page Proof Instructions and Queries

Thank you for choosing to publish with us. This is your final opportunity to ensure your article will be accurate at publication. Please review your proof carefully and respond to the queries using the circled tools in the image below, which are available in Adobe Reader DC* by clicking **Tools** from the top menu, then clicking **Comment**.

Please use *only* the tools circled in the image, as edits via other tools/methods can be lost during file conversion. For comments, questions, or formatting requests, please use ⊤. Please do *not* use comment bubbles/sticky notes ⊙.

*If you do not see these tools, please ensure you have opened this file with **Adobe Reader DC**, available for free at get.adobe.com/reader or by going to Help > Check for Updates within other versions of Reader. For more detailed instructions, please see us.sagepub.com/ReaderXProofs.

Sl. No.	Query
	Please note that we cannot add/amend orcid ids for any article at the proof stage. following orcid's guidelines, the publisher can include only orcid ids that the authors have specifically validated for each manuscript prior to official acceptance for publication.
	Please confirm that all author information, including names, affiliations, sequence, and contact details, is correct.
	Please review the entire document for typographical errors, mathematical errors, and any other necessary corrections; check headings, tables, and figures.
	Please ensure that you have obtained and enclosed all necessary permissions for the reproduction of artworks (e.g. illustrations, photographs, charts, maps, other visual material, etc.) not owned by yourself. please refer to your publishing agreement for further information.
	Please note that this proof represents your final opportunity to review your article prior to publication, so please do send all of your changes now.
	Please confirm that the acknowledgement, funding and conflict of interest statements are accurate.
1	Please check whether the article title is correct as set.
2	Please provide complete address details for the corresponding author.
3	Please check whether all variables/terms/functions/Greeks are accurately and consistently used throughout the article.
4	Please check whether equation citations throughout the article match corresponding equations.
5	Please note that original "Refs 11 and 49" were identical; hence, "Ref. 49" has been deleted and the following references have been renumbered. Please check.
6	Please note that some of the references have been renumbered to make their citations sequential in text. Please check.

Couple-stress effects in a thin film bonded to a half-space==[AQ: 1]==

MA Güler

College of Engineering and Technology, American University of the Middle East, Egaila, Kuwait

Y Alinia (iD)

Department of Mechanical Engineering, Hakim Sabzevari University, Sabzevar, Iran

E Radi (iD)

Department of Sciences and Methods for Engineering, University of Modena and Reggio Emilia, Reggio Emilia, Italy

Abstract

This study investigates the contact mechanics of a thin film laying on an elastic substrate within the context of couple-stress elasticity. It aims to introduce the effects of material internal length scale, which has proven an effective way of modeling structures at micro- to nano-scales, allowing to capture their size-dependent behavior. Specifically, stress analysis for a thin film bonded to a couple-stress elastic half-space is considered under plane strain loading conditions by assuming that both shear stress and couple tractions are exchanged between the thin film and the substrate. The problem is converted to a singular integral equation, which is solved by expanding the shear stress tractions as a Chebyshev series. The results show that the introduction of couple tractions decreases the shear stress tractions and the axial load in the thin film. When the characteristic length is sufficiently small, but still finite, the results for classical elastic behavior are approached.

1. Introduction

Thin film/substrate systems have been extensively used in many industries, including micro/opto–electro–mechanics, aerospace, and automotive applications [1–3]. Their utility is especially valuable in sensors and healthcare devices such as tire pressure sensors [4], wearable health monitoring devices [5–7], optoelectronic lenses [8], thermoelectric generators [9,10], and piezoelectric actuators [11,12]. For

Corresponding author:
E Radi, Department of Sciences and Methods for Engineering, University of Modena and Reggio Emilia, Reggio Emilia, Italy.
Email: enrico.radi@unimore.it==[AQ: 2]==

example, one of the important devices in terms of renewable energy is a thermoelectric device used in waste heat recovery systems [13]. One of the major problems in these systems mentioned above is obtaining a stable interface, which clearly affects the reliability and performance of these devices. Especially the mechanical strength and the debonding failure mechanism are the major issues in obtaining efficient and stable devices. Therefore, understanding the mechanics of the thin film/substrate system is essential in designing the devices mentioned above.

There are two classical approaches to studying the mechanics of thin films: fracture mechanics and contact mechanics. In the fracture mechanics approach, it is usually assumed that there is a pre-existing crack at the interface [14,15] and the failure would be starting due to an interface crack or a transverse crack in the substrate [16,17]. It is also well known that residual stresses due to manufacturing methods can cause failure in the form of edge or buckle delamination [18]. In contact mechanics approach, where it is assumed that there is perfect bonding between the interfaces, the critical issue is estimating the stress field at the interface for crack initiation [19–21]. In this work, we used the contact mechanics approach.

With the advancement of additive manufacturing technologies, thin film/substrate systems gained much attention in micro- and nano-electromechanical systems (MEMS/NEMS) through the applications mentioned above. In MEMS/NEMS, the length scales become comparable to the intrinsic length of the material. This occurrence thus implies the need to consider the issue of size effects. There are various higher-order theories that have been developed that involve higher-order strains in the constitutive equations of the material. The most commonly used ones are the couple-stress theory [22–24] and the strain gradient theory [25–27]. In the couple-stress theory, rotation gradients are introduced in addition to the usual strains considered in the classical theory of elasticity. The related constitutive equations then involve a new length parameter, l, which has a dimension of length that does not exist in the classical theory, e.g., for metals, the internal material length is in the same order of the lattice parameters [28,29], for foam and porous materials, the internal material length is about the average unit cell size, and for laminates, the internal material length is equal to their thickness.

In the last two decades, this enhanced theory has been successfully applied for modeling the size-dependent behavior of contact mechanics problems, such as a two-dimensional (2D) tilted punch [30], 2D cylindrical and wedge indentation [31], 2D indentation problems with various punch profiles [32], and three-dimensional (3D) sphere problem [33]. It has also been applied to fracture mechanics problems such as a plane strain notch [34] and mode III cracks under quasistatic and dynamic propagation [35–37]. Furthermore, it has also been proven to be able to predict size-dependent behavior of micro-sized beam and plate problems, such as functionally graded beams [38], functionally graded Kirchhoff and Mindlin plates [39], micro- and nano-beams [40], and sandwich beams with prismatic cores [41]. It has been also used for modeling the response of thin films film resting on a couple-stress substrate at the microscale in Zhou et al. [42], but only classical tractions and no couple tractions were assumed to be exchanged between the film and the substrate.

Recently, Radi [43] extended the analysis of contact problems by assuming that the interaction occurs also by couple tractions. Under this assumption, he solved the bonded frictionless contact problem for a film/substrate system, where the film is modeled as an Euler–Bernoulli (EB) beam on a couple-stress substrate. He showed that couple-stress tractions have an unusual distribution along the contact zone and have a strong effect on the beam internal forces and moment. He also noted that the size dependency becomes more pronounced if the beam length is comparable to the intrinsic characteristic length of the substrate. Later, Radi et al. [44] extended the same problem by considering the receding contact between the EB beam and the substrate. They concluded that including the size effect in the problem resulted in highly peaked contact pressures near the load application point. Furthermore, they also observed that contact pressure and bending moment are significantly affected when the length scales of the substrate and contact zone are comparable.

In this study, we investigate the size effect in a thin/film substrate system considering couple-stress elasticity. We consider that the right edge of the film is subjected to a tensile load. The main objective of this paper is to study the effects of geometrical parameters and material mismatch between the film and the substrate on the interfacial shear and tensile stresses in the film.

This paper is organized as follows. The governing equations for the thin film/substrate system are provided in section 2 for a tensile load applied at the right end of the film and the problem is reduced to a singular integral equation. The solution procedure of the integral equation based on the Chebyshev
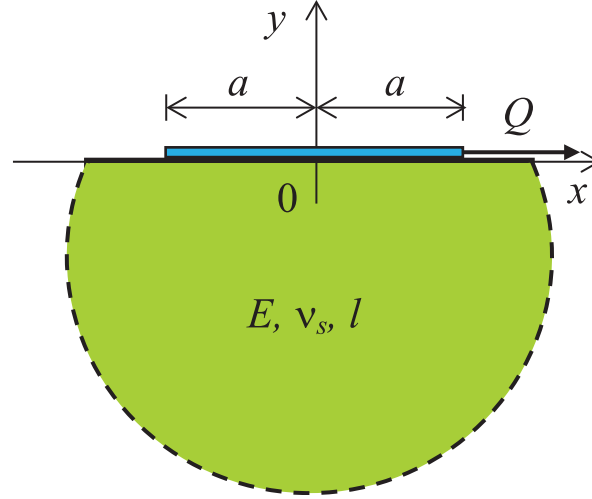
Figure 1. Thin film perfectly bonded on the surface of a couple-stress half-plane, loaded at the right edge by the point load Q.

series expansion is detailed in section 3. The results are presented and discussed in section 4. Finally, the conclusions obtained from this study are reported in section 5.

2. Governing equations

The geometry of the problem for a thin film of length $2a$ and thickness h perfectly bonded to an elastic substrate is shown in Figure 1. A single tensile loading, Q, is applied to the right edge of the film. The size dependency of the substrate is taken into account utilizing the couple-stress theory of elasticity with constrained rotation [45], under plane strain loading conditions. Therefore, the interaction between the film and the substrate is modeled by an interfacial shear stress, $\tau = \tau_{yx}$, and a couple traction, $m = m_{yz}$, along the interface, namely, for $-a < x < a$, while the peeling stress, σ_{yy}, is neglected due to the thin film approximation.

The couple-stress substrate is then characterized by the following strain and curvature fields:[AQ: 3][AQ: 4]

$$\varepsilon_{xx}^s = \frac{\partial u_x}{\partial x}, \ \varepsilon_{yy}^s = \frac{\partial u_y}{\partial y}, \ \varepsilon_{xy}^s = \frac{1}{2}\left(\frac{\partial u_x}{\partial y} + \frac{\partial u_y}{\partial x}\right), \tag{1}$$

$$\kappa_{xz}^s = \frac{\partial \omega_z}{\partial x}, \ \kappa_{yz}^s = \frac{\partial \omega_z}{\partial y}, \tag{2}$$

where

$$\omega_z = \frac{1}{2}\left(\frac{\partial u_y}{\partial x} - \frac{\partial u_x}{\partial y}\right),$$

is the microrotation field, which is constrained to the in-plane displacement field u_x and u_y in the substrate. The balance equations for stress and couple-stress fields, denoted by $\boldsymbol{\sigma}$ and $\boldsymbol{m}$, respectively, read:

$$\frac{\partial \sigma_{xx}^s}{\partial x} + \frac{\partial \sigma_{yx}^s}{\partial y} = 0, \ \frac{\partial \sigma_{xy}^s}{\partial x} + \frac{\partial \sigma_{yy}^s}{\partial y} = 0, \ \sigma_{xy}^s - \sigma_{yx}^s + \frac{\partial m_{xz}^s}{\partial x} + \frac{\partial m_{yz}^s}{\partial y} = 0. \tag{3}$$

For the couple-stress elastic substrate, the constitutive relations between stresses and strains under plane strain loading conditions are the same as for classical linear and isotropic elastic materials, and thus, they are defined by two scalar parameters, namely, the shear modulus μ_s and the Poisson ratio ν_s:
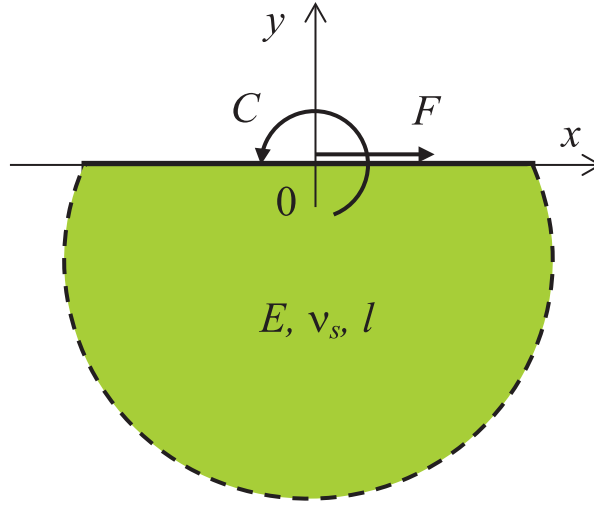
Figure 2. Tangential load F and couple C applied on the surface of a couple-stress half-plane at the origin of the coordinate reference system.

$$\varepsilon_{xx}^s = \frac{1}{2\mu_s}[(1-\nu_s)\sigma_{xx}^s - \nu_s\sigma_{yy}^s],$$

$$\varepsilon_{yy}^s = \frac{1}{2\mu_s}[(1-\nu_s)\sigma_{yy}^s - \nu_s\sigma_{xx}^s],\, , \tag{4}$$

$$\varepsilon_{xy}^s = \frac{1}{2\mu_s}(\sigma_{xy}^s + \sigma_{yx}^s).$$

The constitutive relations between couple stresses and curvatures then introduce the additional microstructural parameter *l*, called material characteristic length, and may be written as:

$$\kappa_{xz}^s = \frac{m_{xz}^s}{4\mu_s l^2}, \kappa_{yz}^s = \frac{m_{yz}^s}{4\mu_s l^2}. \tag{5}$$

2.1. Green's functions for the couple-stress elastic substrate

The tangential displacement u_x at the surface of a couple-stress elastic half-plane due to a concentrated tangential load F and a couple C acting at the origin of the coordinate system (see Figure 2) was provided in Song et al. [46] and Radi [43], respectively, namely:

$$u_x(x,0) = F\frac{1-\nu_s}{\pi\mu_s}\int_0^\infty \frac{\sqrt{1+s^2 l^2}}{s\,g\,(sl)}\cos sx\,ds - C\frac{1-\nu_s}{\pi\mu_s}\int_0^\infty \frac{\sqrt{1+s^2 l^2} - sl}{g\,(sl)}\cos sx\,ds, \tag{6}$$

where

$$g(z) = \sqrt{1+z^2} + 4(1-\nu_s)z^2(\sqrt{1+z^2} - z). \tag{7}$$

Note that the function $g(z)$ behaves as $(3-2\nu_s)\,z + O(z)$ as $z \to \infty$ and consequently, the tangential displacement u_x under the loading couple is finite. The corresponding axial strain along the half-plane surface then follows from the derivative of the displacement equation (7) with respect to the variable *x* as:
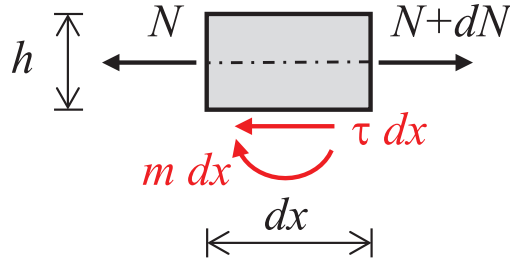
Figure 3. Free body diagram of forces and couples acting on any infinitesimal thin film element of thickness *h*.

$$\varepsilon_{xx}^s(x, 0) = - F \frac{1 - \nu_s}{\pi \mu_s} \int_0^\infty \frac{\sqrt{1 + s^2 l^2}}{g\,(sl)} \sin sx \, ds + C \frac{1 - \nu_s}{\pi \mu_s} \int_0^\infty \frac{\sqrt{1 + s^2 l^2} - sl}{g\,(sl)} s \sin sx \, ds. \tag{8}$$

2.2. Longitudinal strain in the elastic thin film

The balance equations for the thin film require (Figure 3):

$$\tau(x) = N'(x), m(x) = \tau(x)h/2, \tag{9}$$

where $\tau(x)$ and $m(x)$ are the shear tractions and couple tractions exchanged between the thin film and the couple-stress substrate, N is the axial load in the thin film, and the prime denotes the derivative with respect to x. The axial load in the thin film follows from integration of equation (9)₁ between $-a$ and x, using the boundary conditions $N(-a) = 0$, namely:

$$N(x) = \int_{-a}^x \tau(t) \, dt. \tag{10}$$

For the whole film, one has:

$$Q = \int_{-a}^a \tau(t) \, dt, \tag{11}$$

where Q is the concentrate load applied at the right edge of the film. Then, the axial strain along the film under plane strain loading conditions is given by:

$$\varepsilon_{xx}^f(x) = \frac{1 - \nu_f^2}{E_f h} N(x) = \frac{1 - \nu_f^2}{E_f h} \int_{-a}^x \tau(t) \, dt, \tag{12}$$

where E_f and ν_f are the elastic Young modulus and the Poisson ratio of the elastic thin film, respectively.

2.3. Strain compatibility conditions for perfectly bonded contact

Let us now consider a thin film of length $2a$ and thickness $h << a$ perfectly bonded to the couple-stress substrate (Figure 3), under plane strain conditions. Using the Green function equation (8), we can easily obtain the surface strain on the top of the substrate in terms of the shear stress distribution $\tau(x)$ and couple tractions $m(x)$ exchanged between the thin film and the substrate:

$$\varepsilon_{xx}^s(x,0) = \frac{1-\nu_s}{\pi \mu_s}\left\{-\int_{-a}^{a}\tau(t)\,dt\int_{0}^{\infty}\frac{\sqrt{1+s^2l^2}}{g(sl)}\sin[s\,(x-t)]\,ds + \int_{-a}^{a}m(t)dt\int_{0}^{\infty}\frac{\sqrt{1+s^2l^2}-sl}{g(sl)}\,s\sin[s\,(x-t)]\,ds\right\}, \quad (13)$$

where μ and ν are the shear elastic modulus and the Poisson coefficient of the couple-stress substrate, respectively. The introduction of the balance equation $(9)_1$ then yields:

$$\varepsilon_{xx}^s(x,0) = -\frac{1-\nu_s}{2\pi \mu_s}\int_{-a}^{a}\tau(t)\,dt\int_{0}^{\infty}\frac{2\sqrt{1+s^2l^2}+(\sqrt{1+s^2l^2}-sl)\,sh}{g(sl)}\sin[s\,(x-t)]\,ds. \quad (14)$$

The compatibility conditions along the interface between the film and the substrate then require:

$$\varepsilon_{xx}^s(x,0) = \varepsilon_{xx}^f(x),$$

namely, using equations (12) and (14):

$$\frac{\lambda}{2h}\int_{-a}^{x}\tau(t)\,dt + \frac{1}{2\pi}\int_{-a}^{a}\tau(t)\,dt\int_{0}^{\infty}\frac{2\sqrt{1+s^2l^2}+(\sqrt{1+s^2l^2}-sl)\,sh}{g(sl)}\sin[s\,(x-t)]\,ds = 0, \quad (15)$$

where

$$\lambda = \frac{\mu_s(1-\nu_f)}{\mu_f(1-\nu_s)}, \quad (16)$$

is a non-dimensional parameter.

To single out the most relevant terms as s tends to infinity in the kernel function of the integral equation (15), an asymptotic expansion of the kernel function is performed:

$$\frac{2\sqrt{1+s^2l^2}+(\sqrt{1+s^2l^2}-sl)\,sh}{g(sl)} = \frac{2}{3-2\nu_s} + \frac{h}{2(3-2\nu_s)\,sl^2} + O\left(\frac{1}{s^2}\right), \text{ as } s\to\infty. \quad (17)$$

Then, using the following results [47]:

$$\int_{0}^{\infty}\sin sx\,ds = \frac{1}{x}, \quad \int_{0}^{\infty}\frac{\sin sx}{s}\,ds = \frac{\pi}{2}\,\mathrm{sgn}x, \quad (18)$$

and introducing the non-dimensional quantities:

$$H = h/a, \qquad \Lambda = l/a, \qquad z = sa, \qquad \xi = x/a, \qquad \eta = t/a, \quad (19)$$

the governing integral equation (15) can be rewritten as:

$$\frac{\lambda}{2H}\int_{-1}^{\xi}\tau(\eta)\,d\eta + \int_{-1}^{1}k(\xi-\eta)\tau(\eta)\,d\eta + \frac{1}{\pi(3-2\nu_s)}\int_{-1}^{1}\frac{\tau(\eta)}{\xi-\eta}\,d\eta + \frac{H}{8(3-2\nu_s)\Lambda^2}$$

$$\left[\int_{-1}^{\xi}\tau(\eta)d\eta - \int_{\xi}^{1}\tau(\eta)d\eta\right] = 0, \quad (20)$$

where

$$k(\xi) = \frac{1}{2\pi} \int\limits_0^\infty \left[\frac{(2 + z\,H)\,\sqrt{1 + z^2\Lambda^2} - z^2\Lambda H}{g(z\Lambda)} - \frac{2}{3 - 2\nu_s} - \frac{H}{2\,(3 - 2\nu_s)\Lambda^2 z} \right] \sin z\xi\, dz, \tag{21}$$

or equivalently, after some manipulation:

$$k(\xi) = \frac{1}{2\pi\,(3 - 2\nu_s)} \int\limits_0^\infty \left[4(1 - \nu_s) - \frac{H}{2\Lambda^2 z} \right] \frac{(1 - 2\Lambda^2 z^2)\,\sqrt{1 + \Lambda^2 z^2} + 2\Lambda^3 z^3}{g(z\Lambda)} \sin z\xi\, dz. \tag{22}$$

2.4. Limit behavior for vanishing characteristic length

In the limit as l tends to zero, from equation (15), one has:

$$\frac{\lambda}{2h} \int\limits_{-a}^x \tau(t)\, dt + \frac{1}{\pi} \int\limits_{-a}^a \tau(t)\, dt \int\limits_0^\infty \left(1 + \frac{sh}{2} \right) \sin[s\,(x - t)]\, ds = 0. \tag{23}$$

Then, using equation (18), one obtains:

$$\frac{\lambda}{2h} \int\limits_{-a}^x \tau(t)\, dt + \frac{1}{\pi} \int\limits_{-a}^a \frac{\tau(t)}{x - t}\, dt + \frac{h}{2\pi} \int\limits_0^\infty s\, ds \int\limits_{-a}^a \tau(t)\, \sin[s\,(x - t)]\, dt = 0. \tag{24}$$

The last term in equation (24) is not present in the integral equation governing the contact problem between a film and a classical elastic substrate [20] and is due to the contribution of the couple stress to the balance equation according to equation (9)$_2$. It can be neglected as the film thickness h tends to zero, which is the usual hypothesis adopted for a thin film. Indeed, the applied load is balanced by the interfacial shear tractions with no need for couple tractions or bending moment in the beam only for $h = 0$.

3. Approximated solution

At the edges of the contact, namely, at $x = \pm a$, the shear stress τ is expected to display square root singularity. Accordingly, we represent the shear stress using a series of Chebyshev polynomials of the first kind T_n, namely:

$$\tau(\eta) = \frac{Q}{2a} \sum_{n=0}^\infty c_n \frac{T_n(\eta)}{\sqrt{1 - \eta^2}}, \quad \text{for}\,|\eta| \leqslant 1, \tag{25}$$

where the coefficients c_n ($n = 0, 1, 2, \ldots$) can be determined using a collocation method as described in the following. According to equation (9)$_2$, the couple tractions m also display square root singular behavior at the edges of the contact zone.

The introduction of representations equation (25) in the balance condition equation (11) provides the first coefficient of the series expansion equation (25):

$$c_0 = 2/\pi. \tag{26}$$

A similar substitution in the integral equation (20), using the following identities:

$$\int\limits_{-1}^1 \frac{T_n(\eta)\, d\eta}{(\xi - \eta)\,\sqrt{1 - \eta^2}} = \begin{cases} 0 & \text{for } n = 0, \\ -\pi\, U_{n-1}(\xi), & \text{for } n \geqslant 1, \end{cases} \tag{27}$$

$$\int_{-1}^{\xi} \frac{T_n(\eta)\, d\eta}{\sqrt{1 - \eta^2}} = \begin{cases} \pi - \arccos \xi, & \text{for } n = 0, \\ -U_{n-1}(\xi)\sqrt{1 - \xi^2}/n, & \text{for } n \geqslant 1, \end{cases} \tag{28}$$

$$\int_{\xi}^{1} \frac{T_n(\eta)\, d\eta}{\sqrt{1 - \eta^2}} = \begin{cases} \arccos \xi, & \text{for } n = 0, \\ U_{n-1}(\xi)\sqrt{1 - \xi^2}/n, & \text{for } n \geqslant 1, \end{cases} \tag{29}$$

for $-1 \leqslant \xi \leqslant 1$, then yields the following equation for the unknown parameters c_n, for $n = 1, 2, ..., K$:

$$\sum_{n=1}^{\infty} c_n \left\{ \int_{-1}^{1} k(\xi - \eta) \frac{T_n(\eta)}{\sqrt{1 - \eta^2}}\, d\eta - \left[\frac{1}{3 - 2\nu_s} + \left(\frac{H}{2(3 - 2\nu_s)\Lambda^2} + \frac{\lambda}{H} \right) \frac{\sqrt{1 - \xi^2}}{2n} \right] U_{n-1}(\xi) \right\}$$
$$+ \frac{2}{\pi} \int_{-1}^{1} \frac{k(\xi - \eta)}{\sqrt{1 - \eta^2}}\, d\eta + \frac{\lambda}{H} \left(1 - \frac{\arccos \xi}{\pi} \right) + \frac{H}{2(3 - 2\nu_s)\Lambda^2} \left(\frac{1}{2} - \frac{\arccos \xi}{\pi} \right) = 0, \tag{30}$$

which holds for $-1 \leqslant \xi \leqslant 1$.

3.1. Collocation procedure

A linear and homogeneous system of K algebraic equations for the unknown coefficients c_n (for $n = 1$, $2, ..., K$) is derived from the strain compatibility condition equation (30) by truncating the series equation (25) to the first $K + 1$ terms and, correspondingly, evaluating equation (30) at K collocation points ξ_k ($k = 1, 2, ..., K$), ranging between -1 and 1, selected as the positive roots of the Chebyshev polynomial $T_{2K}(\xi)$, namely:

$$\xi_k = \cos \frac{(2k - 1)\pi}{2K}, \text{ for } k = 1, 2, \ldots, K. \tag{31}$$

Moreover, the definite integrals in equation (30) are calculated using the Gauss Chebyshev quadrature with M nodes η_j ($j = 1, 2, ..., M$) coinciding with the roots of the Chebyshev polynomial $T_M(\eta)$, namely:

$$\eta_j = \cos \frac{(2j - 1)\pi}{2M}, \text{ for } j = 1, 2, \ldots, M. \tag{32}$$

Then, equation (32) provides the following system of K algebraic equations for the K unknown coefficients c_n for $n = 1, 2, ..., K$:

$$\sum_{n=1}^{K} c_n \left\{ \frac{\pi}{M} \sum_{j=1}^{M} k(\xi_k - \eta_j) T_n(\eta_j) - \left[\frac{2}{3 + \kappa} + \left(\frac{H}{2(3 - 2\nu_s)\Lambda^2} + \frac{\lambda}{H} \right) \frac{\sqrt{1 - \xi_k^2}}{2n} \right] U_{n-1}(\xi_k) \right\}$$
$$+ \frac{2}{M} \sum_{j=1}^{M} k(\xi_k - \eta_j) + \frac{\lambda}{H} \left(1 - \frac{\arccos \xi_k}{\pi} \right) + \frac{H}{2(3 - 2\nu_s)\Lambda^2} \left(\frac{1}{2} - \frac{\arccos \xi_k}{\pi} \right) = 0, \tag{33}$$

for $k = 1, 2, ..., K$. Once the coefficients c_n, for $n = 0, 2, ..., K$, are known, the interfacial shear stress is given by equation (25) and the axial load in the thin film follows from equations (10) and (25) as:

$$N(\xi) = \frac{Q}{2} \sum_{n=0}^{K} c_n \int_{-1}^{\xi} \frac{T_n(\eta)}{\sqrt{1 - \eta^2}}\, d\eta = Q \left[1 - \frac{\arccos \xi}{\pi} - \sum_{n=1}^{\infty} \frac{c_n}{2n} U_{n-1}(\xi) \sqrt{1 - \xi^2} \right]. \tag{34}$$
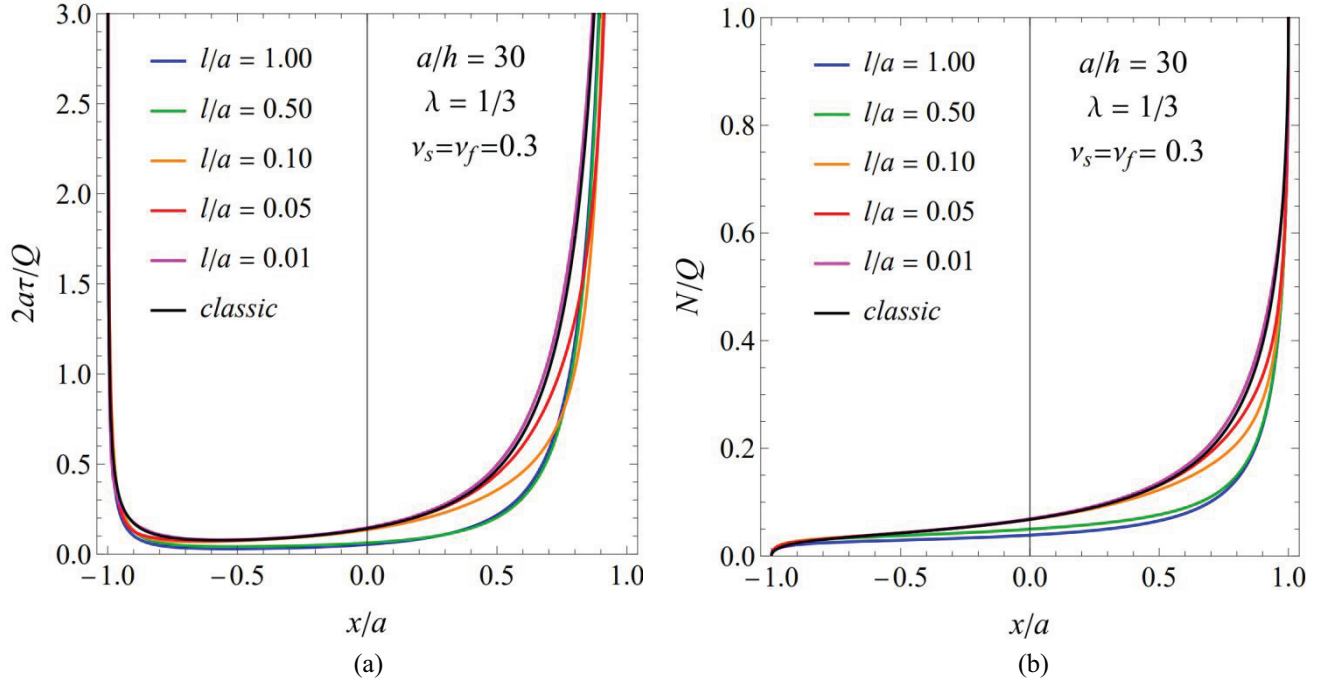
Figure 4. Normalized distributions of the interfacial shear stress along the interface (a) and axial load in the film (b) for various values of the characteristic length ratio *l/a* and for classical elastic behavior of the substrate (for *a/h* = 30, λ = 1/3, $v_s = v_f = 0.3$).

Then, the tensile axial stress in the thin film is given by:

$$\sigma_{xx}^f(x) = \frac{N(x)}{h}. \tag{35}$$

3.2. Strength of stress singularities

Let $k_1(a)$ and $k_1(-a)$ denote the strength of the shear stress singularity at the right and left ends of the thin film, respectively, which are defined by:

$$k_1(a) = \lim_{x \to a} \sqrt{2(a-x)}\,\tau(x),\; k_1(-a) = \lim_{x \to -a} \sqrt{2(a+x)}\,\tau(x). \tag{36}$$

By introducing representations equation (25) for the shear stress, they can be calculated in normalized form as:

$$k_1^*(a) = \frac{2a}{Q} k_1(a) = \sum_{n=0}^K c_n,\; k_1^*(-a) = \frac{2a}{Q} k_1(-a) = \sum_{n=0}^K (-1)^n c_n. \tag{37}$$

4. Results

In the following results, we assumed the same Poisson's ratio both for the film and substrate to be $v_s = 0.3$ and we used $K \geqslant 40$ collocation points.

The effect of the size parameter, *l/a*, on the normalized interfacial shear stress, $2a\tau/Q$, and axial load, *N/Q*, is shown in Figure 4. The shear stress distribution along the contact zone, namely, for $-a < x < a$, is not symmetric for the classical elasticity solution and attains much higher values near the right edge of the film, namely, where the external load *Q* is applied. Introducing the size effect, the asymmetry of
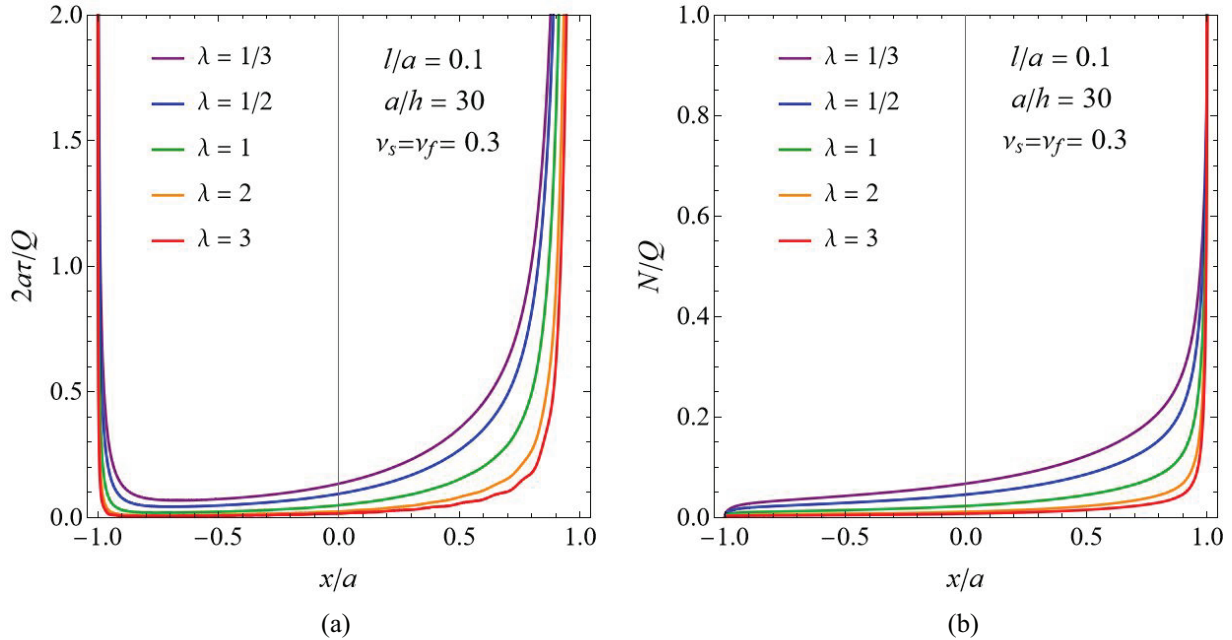
Figure 5. Normalized distributions of the interfacial shear stress along the interface (a) and axial load in the film (b) for various values of the stiffness parameter λ (for $a/h = 30$, $l/a = 0.1$, $\nu_s = \nu_f = 0.3$).

the shear stress distribution is reduced and the shear stress magnitude near the right edge is much lower compared to the classical solution. Due to the effects of the non-classical behavior of the substrate, the axial load in the film decreases as the material characteristic length increases. There are no significant changes in the interfacial shear or axial load in the film for $l/a > 0.5$. Moreover, the results approach the classical elastic solution for a small but finite value of the characteristic length, thus validating the present approach.

Figure 5 depicts the effect of the stiffness ratio parameter λ on the film shear stress and the axial load for the characteristic length ratio $l/a = 0.1$ and the geometric parameter $a/h = 30$. It can be observed that, as the stiffness of the substrate gets stiffer than the film, namely, for $\lambda > 1$, both the shear stress and the axial load in the film decrease very fast out of the loaded film edge. This is also observed in the related studies (see, e.g., [20,11,48,49]). The reason for this phenomenon may be attributed to the fact that when $\lambda > 1$ (a soft film on a stiff substrate), the more compliant substrate eventually deforms to relieve interfacial shear and normal stresses in the film [49]. On the contrary, when $\lambda < 1$ (a stiff film on a soft substrate), the stresses get much higher as the stiffness ratio parameter decreases.

The effect of the film length on the film shear stresses is illustrated in Figure 6(a) for the characteristic length ratio $l/a = 0.1$ and the stiffness ratio, $\lambda = 1/3$. It is concluded that as the film gets thinner, the interfacial shear stresses get smaller and the skewness of the shear stress distribution decreases (compare the red and the black lines in Figure 6(a), corresponding to $a/h = 100$ and $a/h = 10$, respectively). This behavior is also observed in the literature [49–51]. Note that as the film gets thicker or a/h decreases, the axial load on the film increases leading to an increase in the interfacial shear stresses (see Figure 6(a) and (b)).

Figures 7 and 8 provide results similar to those obtained in Figures 4 and 6 but for the parameter $\lambda = 2$ instead of $\lambda = 1/3$, namely, for a more compliant film. In this case, the interfacial shear stress and the axial load along the film are much smaller than those observed in Figures 4 and 6 for $\lambda = 1/3$. In particular, for a very thin film, namely, for $a/h \geqslant 50$, the load Q is almost fully transmitted to the ground at very short distance from the loaded film end, where it displays singular behavior. Therefore, the interfacial shear stress exhibits a very rapid variation near the loaded film end. Due to this occurrence, the
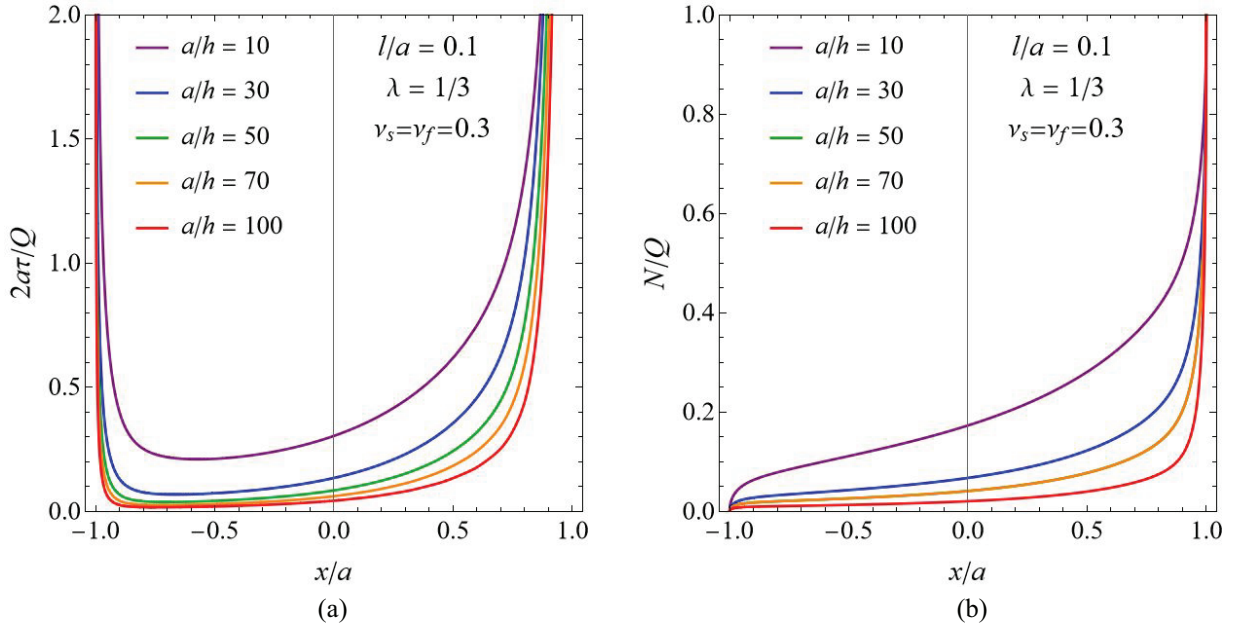
Figure 6. Normalized distributions of the interfacial shear stress along the interface (a) and axial load in the film (b) for various values of the geometric ratio *a/h* (for $\lambda = 1/3$, *l/a* = 0.1, $v_s = v_f = 0.3$).
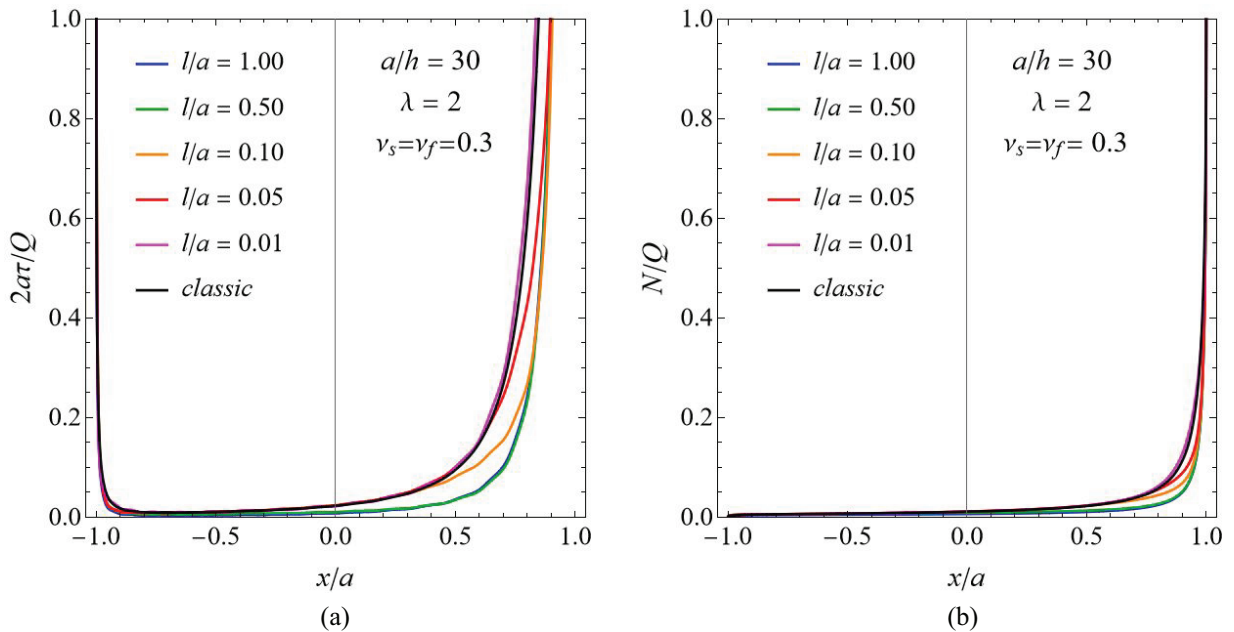

Figure 7. Normalized distributions of the interfacial shear stress along the interface (a) and axial load in the film (b) for various values of the characteristic length ratio *l/a* and for classical elastic behavior of the substrate (for *a/h* = 30, $\lambda = 2$, $v_s = v_f = 0.3$).
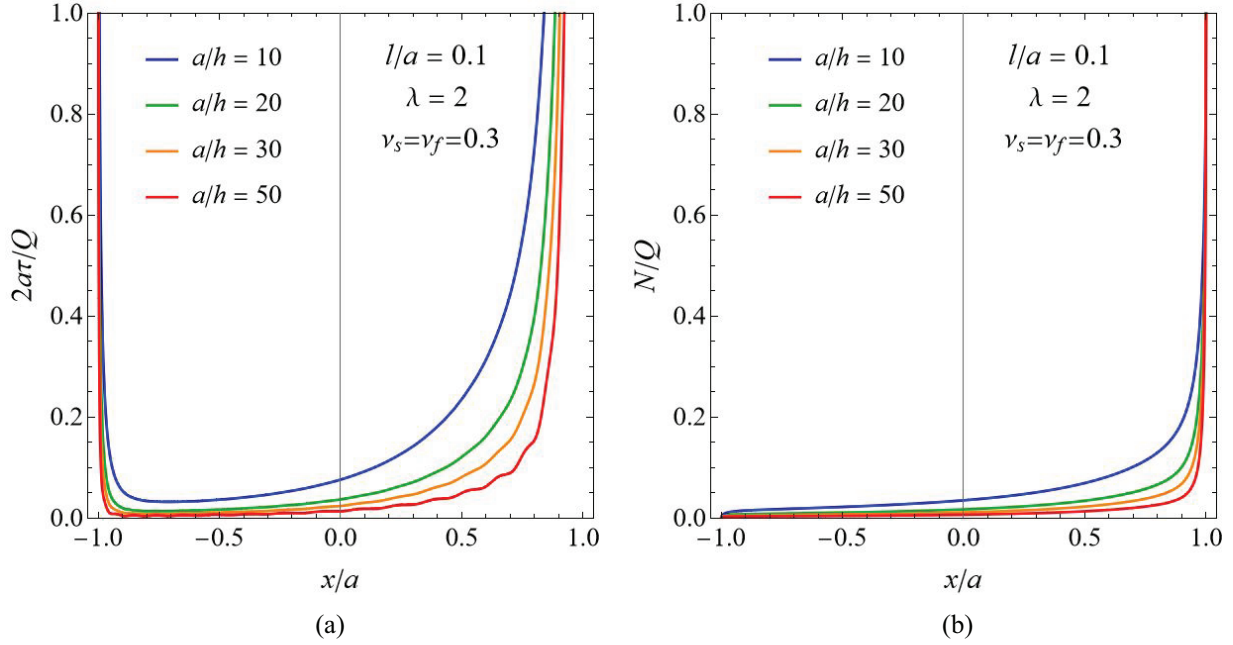
Figure 8. Normalized distributions of the interfacial shear stress along the interface (a) and axial load in the film (b) for various values of the geometric ratio a/h (for $\lambda = 2$, $l/a = 0.1$, $\nu_s = \nu_f = 0.3$).

results obtained by Chebyshev series expansion of the shear stress provided in Figure 8(a) display oscillatory behavior near the loaded end, as a consequence of the Gibbs phenomenon. To mitigate this effect, we introduced the Lanczos sigma factors [52] in the finite series expansion of the shear stress, as suggested in Crouch and Mogilevskaya [53], namely:

$$\tau(\eta) = \frac{Q}{2a} \sum_{n=0}^{K} c_n \frac{T_n(\eta)}{\sqrt{1 - \eta^2}} \frac{K}{n\pi} \sin \frac{n\pi}{K}, \text{for} |\eta| \leqslant 1. \tag{38}$$

Finally, the variations of the strength of stress singularity are presented in Figure 9 by varying the characteristic length (Figure 9(a)), the stiffness ratio λ (Figure 9(b)), and the film aspect ratio a/h (Figure 9(c)). Since the load is applied at the right end of the film, namely, at $x/a = 1$, it is obvious that the strength of stress singularity is considerably lower at the left end as compared to the right end. Moreover, the strength of singularity at the loaded end significantly increases for large value of the stiffness parameter λ, namely, for compliant behavior of the film, as observed in Figures 7 and 8.

For classical elastic behavior of the substrate and for $a/h = 30$ and $\lambda = 1/3$, the normalized strength of stress singularity for the loaded end is $k_1^*(a) = 3.568$ and for the free end is $k_1^*(-a) = 0.136$. These values are recovered by the couple-stress model of the substrate for a small but finite value of the characteristic length l, as illustrated in Figure 9(a). However, both ends display a much smaller strength of the stress singularity as l tends to zero. Indeed, the present model does not provide significant results for an almost null characteristic length, at least for a finite film thickness. This discrepancy between the classical elastic solution and the response of the present model for $l \cong 0$ is due to the last term in equation (24), which is not present in the classical elastic contact problem, but it appears here for a finite film thickness. Indeed, for $l = 0$, the couple tractions also vanish along the interface, then for a finite film thickness $h > 0$, the balance condition equation $(9)_2$ cannot be satisfied unless $\tau(x) = 0$ or a bending moment takes place within the film.
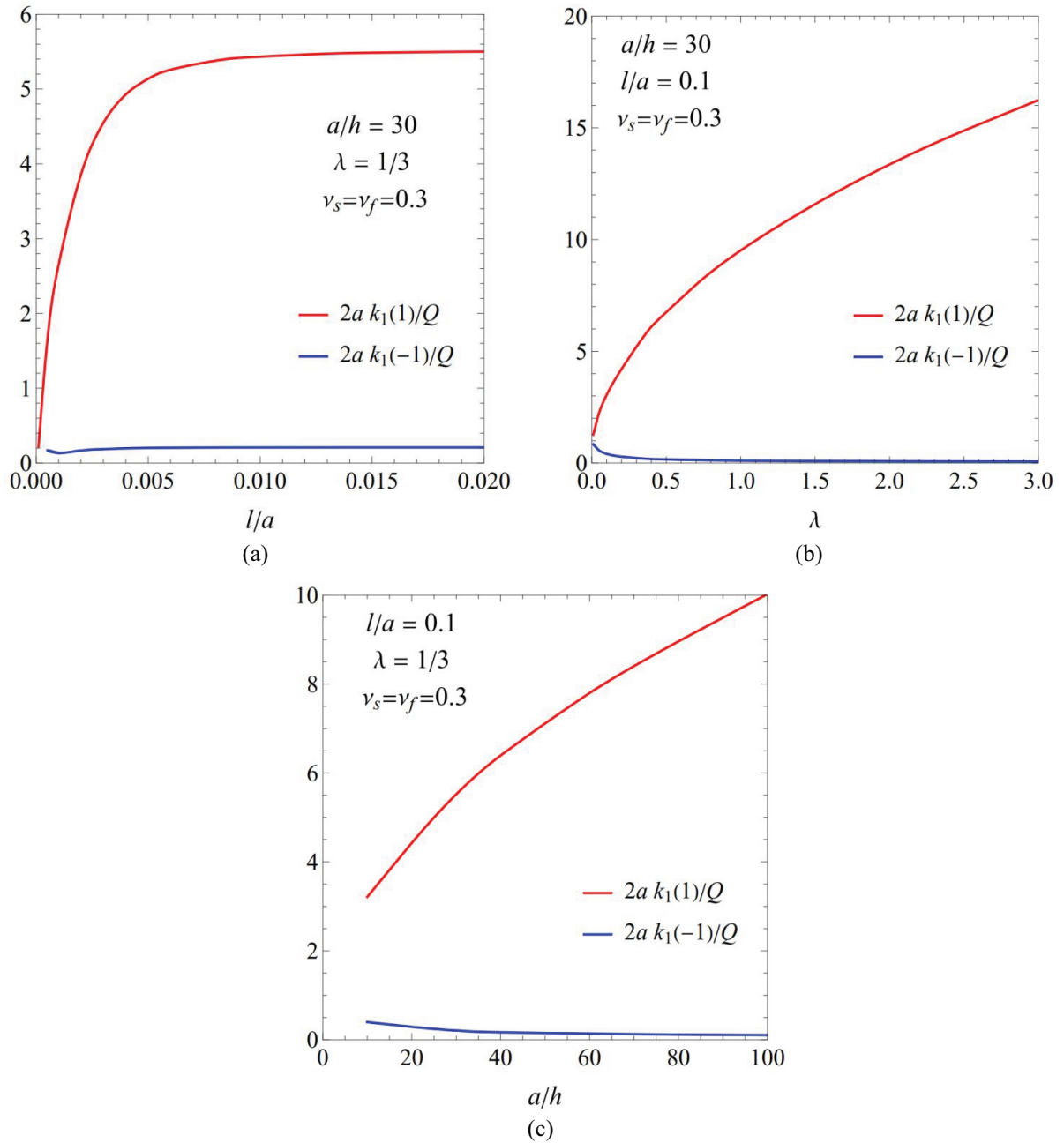
Figure 9. Variations of the strength of stress singularities (a) with the characteristic length ratio l/a, (b) with the stiffness parameter λ, and (c) with the geometric ratio a/h, ($\nu_s = \nu_f = 0.3$).

Conclusion

This work presents an analytical model based on the Chebyshev series expansions to investigate the contact problem between a thin elastic film under tension and a couple-stress elastic substrate.

The most important features of this study are as follows:

- The capability to calculate shear and couple tractions along the interface, the axial stress at any point in the thin film, and the strength of stress singularity at the film ends.
- The fulfillment of the balance and compatibility equations in the thin film and the substrate.

- The use of Chebyshev series expansions for solving a singular integral equation instead of purely numerical procedures.
- The parametric nature of the analysis and the possibility of using it for any geometry and constitutive behavior of the film and substrate.
- The capability of the model to account for the film thickness in the balance equation of the film.

This research demonstrated that accounting for non-classical and size-dependent behavior of the substrate as well as for couple tractions provides a remarkable reduction of the axial load and axial stress within the thin film. Moreover, the results obtained from the present model agree well with the classical elastic solution for a relatively small characteristic length, thus validating the present approach. However, the present model does not provide representative results for a null characteristic length, at least for a finite film thickness.

As expected, in the asymmetrically loaded thin film considered here, the magnitude of the shear stress along the interface is considerably larger on the loaded edge than on the free edge. Furthermore, according to the obtained results, the couple tractions are significant compared to the shear stress tractions, especially for thicker films, and must be considered in the investigations if the substrate is micropolar and size dependent.

ORCID iDs

Y Alinia https://orcid.org/0000-0001-8475-7382
E Radi https://orcid.org/0000-0002-7410-3008

References[AQ: 5][AQ: 6]

[1] Subrahmanyam, V, Narayana Rao, PSS, Ramamurthy, DV, et al. Nano/micro-electro-mechanical systems for sensor applications: a brief review. *IETE J Educ* 2010; 51: 23–31.
[2] Vajire, SL, Singh, AP, Saini, DK, et al. Novel machine learning-based prediction approach for nanoindentation load-deformation in a thin film: applications to electronic industries. *Comput Ind Eng* 2022; 174: 108824.
[3] Wang, Y, Li, Z, and Xiao, J. Stretchable thin film materials: fabrication, application, and mechanics. *J Electron Packag* 2016; 138: 020801.
[4] Matsuzaki, R, and Todoroki, A. Wireless flexible capacitive sensor based on ultra-flexible epoxy resin for strain measurement of automobile tires. *Sens Actuators A: Phys* 2007; 140: 32–42.
[5] Yin, MJ, Yin, Z, Zhang, Y, et al. Micropatterned elastic ionic polyacrylamide hydrogel for low-voltage capacitive and organic thin-film transistor pressure sensors. *Nano Energy* 2019; 58: 96–104.
[6] Nie, B, Li, R, Cao, J, et al. Flexible transparent iontronic film for interfacial capacitive pressure sensing. *Adv Mater* 2015; 27: 6055–6062.
[7] Joo, Y, Yoon, J, Ha, J, et al. Highly sensitive and bendable capacitive pressure sensor and its application to 1 V operation pressure-sensitive transistor. *Adv Electron Mater* 2017; 3(4): 1600455.
[8] Freund, LB, and Suresh, S. *Thin film materials: stress, defect formation and surface evolution*. Cambridge: Cambridge University Press, 2004.
[9] He, R, Schierning, G, and Nielsch, K. Thermoelectric devices: a review of devices, architectures, and contact optimization. *Adv Mater Technol* 2018; 3: 1700256.

[10] Li, D, Chen, P, Huang, Z, et al. The interfacial behavior of a thermoelectric thin-film bonded to an orthotropic substrate. *Int J Solids Struct* 2023; 267: 112160.

[11] Chen, P, Peng, J, Chen, Z, et al. On the interfacial behavior of a piezoelectric actuator bonded to a homogeneous half plane with an arbitrarily varying graded coating. *Eng Fract Mech* 2019; 220: 106645.

[12] Chen, P, Chen, S, Liu, H, et al. The interface behavior of multiple piezoelectric films attaching to a finite-thickness gradient substrate. *J Appl Mech* 2020; 87: 011003.

[13] Elsheikh, MH, Shnawah, DA, Sabri, MFM, et al. A review on thermoelectric renewable energy: principle parameters that affect their performance. *Renew Sustain Energy Rev* 2014; 30: 337–355.

[14] Akisanya, AR, and Fleck, N. The edge cracking and decohesion of thin films. *Int J Solids Struct* 1994; 31: 3175–3199.

[15] Yu, HH, He, M, and Hutchinson, J. Edge effects in thin film delamination. *Acta Mater* 2001; 49: 93–107.

[16] Sobol, B, Soloviev, A, and Krasnoschekov, A. The transverse crack problem for elastic bodies stiffened by thin elastic coating. *ZAMM J Appl Math Mech* 2015; 95: 1302–1314.

[17] Krasnoshchekov, A, and Sobol, B. Equilibrium of an internal transverse crack in a semiinfinite elastic body with thin coating. *Mech Solids* 2016; 51: 114–126.

[18] Balint, D, and Hutchinson, J. Mode II edge delamination of compressed thin films. *J Appl Mech* 2001; 68: 725–730.

[19] Erdogan, F, and Ozturk, M. On the singularities in fracture and contact mechanics. *J Appl Mech* 2008; 75: 051111.

[20] Guler, MA. Mechanical modeling of thin films and cover plates bonded to graded substrates. *J Appl Mech* 2008; 75: 051105.

[21] Peijian, C, Shaohua, C, and Yin, Y. Nonslipping contact between a mismatch film and a finite-thickness graded substrate. *J Appl Mech* 2016; 83: 021007.

[22] Mindlin, R, and Tiersten, H. Effects of couple-stresses in linear elasticity. *Arch Ration Mech Anal* 1962; 11: 415–448.

[23] Toupin, RA. Elastic materials with couple-stresses. *Arch Ration Mech Anal* 1962; 11: 385–414.

[24] Toupin, RA. Theories of elasticity with couple-stress. *Arch Ration Mech Anal* 1964; 17: 85–112.

[25] Mindlin, RD. Micro-structure in linear elasticity. *Arch Ration Mech Anal* 1964; 16: 51–78.

[26] Mindlin, RD. Second gradient of strain and surface-tension in linear elasticity. *Int J Solids Struct* 1965; 1: 417–438.

[27] Lam, DC, Yang, F, Chong, A, et al. Experiments and theory in strain gradient elasticity. *J Mech Phys Solids* 2003; 51: 1477–1508.

[28] Zhang, X, and Sharma, P. Size dependency of strain in arbitrary shaped anisotropic embedded quantum dots due to nonlocal dispersive effects. *Phys Rev B Condens Matter* 2005; 72: 1953445.

[29] Liu, D, He, Y, Tang, X, et al. Size effects in the torsion of microscale copper wires: experiment and analysis. *Scr Mater* 2012; 66: 406–409.

[30] Gourgiotis, P, Zisis, T, and Baxevanakis, K. Analysis of the tilted flat punch in couple-stress elasticity. *Int J Solids Struct* 2016; 85: 34–43.

[31] Gourgiotis, P, and Zisis, T. Two-dimensional indentation of microstructured solids characterized by couple-stress elasticity. *J Strain Anal Eng Des* 2016; 51: 318–331.

[32] Karuriya, AN, and Bhandakkar, TK. Plane strain indentation on finite thickness bonded layer in couple stress elasticity. *Int J Solids Struct* 2017; 108: 275–288.

[33] Wang, Y, Zhang, X, Shen, H, et al. Couple stress-based 3D contact of elastic films. *Int J Solids Struct* 2020; 191: 449–463.

[34] Gourgiotis, P, and Georgiadis, H. The problem of sharp notch in couple-stress elasticity. *Int J Solids Struct* 2011; 48: 2630–2641.

[35] Radi, E. Effects of characteristic material lengths on mode III crack propagation in couple stress elastic-plastic materials. *Int J Plasticity* 2007; 23: 1439–1456.

[36] Radi, E. On the effects of characteristic lengths in bending and torsion on mode III crack in couple stress elasticity. *Int J Solids Struct* 2008; 45: 3033–3058.

[37] Nobili, A, Radi, E, and Vellender, A. Diffraction of antiplane shear waves and stress concentration in a cracked couple stress elastic material with micro inertia. *J Mech Phys Solids* 2019; 124: 663–680.

[38] Reddy, J. Microstructure-dependent couple stress theories of functionally graded beams. *J Mech Phys Solids* 2011; 59: 2382–2399.

[39] Thai, HT, and Choi, DH. Size-dependent functionally graded Kirchhoff and Mindlin plate models based on a modified couple stress theory. *Compos Struct* 2013; 95: 142–153.

[40] Awrejcewicz, J, Krysko, V, Pavlov, S, et al. Mathematical model of a three-layer micro-and nano-beams based on the hypotheses of the Grigolyuk–Chulkov and the modified couple stress theory. *Int J Solids Struct* 2017; 117: 39–50.

[41] Goncalves, BR, and Romanoff, J. Size-dependent modelling of elastic sandwich beams with prismatic cores. *Int J Solids Struct* 2018; 136: 28–37.

[42] Zhou, YT, Tian, XJ, and Ding, SH. Microstructure size-dependent contact behavior of a thermoelectric film bonded to an elastic substrate with couple stress theory. *Int J Solids Struct* 2022; 256: 111982.

[43] Radi, E. A loaded beam in full frictionless contact with a couple stress elastic half-plane: effects of non-standard contact conditions. *Int J Solids Struct* 2021; 232: 111175.

[44] Radi, E, Nobili, A, and Guler, M. Indentation of a free beam resting on an elastic substrate with an internal lengthscale. *Eur J Mech A Solids* 2022; 10: 104804.

[45] Koiter, W. Couple stresses in the theory of elasticity. Parts I and II. *Nederl Akad Wetensch Proc Ser B* 1964; 67: 17–29.

[46] Song, HX, Ke, LL, and Wang, YS. Sliding frictional contact analysis of an elastic solid with couple stresses. *Int J Mech Sci* 2017; 133: 804–816.

[47] Watanabe, K. *Integral transform techniques for Green's function* (Lecture Notes in Applied and Computational Mechanics). 2nd ed. New York: Springer, 2015.

[48] Chen, P, Peng, J, Yu, L, et al. The interfacial analysis of a film bonded to a finite thickness graded substrate. *Int J Solids Struct* 2017; 120: 57–66.

[49] Abbaszadeh-Fathabadi, SA, Alinia, Y, and Güler, MA. On the mechanics of a double thin film on a finite thickness substrate. *Int J Solids Struct* 2023; 279: 112349.

[50] Chen, P, Chen, S, Guo, W, et al. The interface behavior of a thin piezoelectric film bonded to a graded substrate. *Mech Mater* 2018; 127: 26–38.

[51] Alinia, Y, Abbaszadeh-Fathabadi, SA, and Guler, MA. Stress analysis for a thin film bonded to an orthotropic substrate under thermal loading. *Mech Res Commun* 2020; 109: 103594.

[52] Lanczos, C. *Applied analysis*. Englewood Cliffs, NJ: Prentice Hall, 1956.

[53] Crouch, SL, and Mogilevskaya, SG. Loosening of elastic inclusions. *Int J Solids Struct* 2006; 43: 1638–1668.